Volume 4 Issue 2 (September 2024)
DOI 10.24191/jaeds.v4i2.79
eISSN 2805-5756

Journal of Applied Engineering Design & Simulation

Modelling and Simulation of Cyclic Nanoindentation for Y-TZP Ceramic

S.K.H. Baharudin and J. Saedon*
College of Engineering, Universiti Teknologi MARA, Shah Alam 40450 Selangor, Malaysia.
*corresponding author: jurisaedon41@uitm.edu.my

ABSTRACT

Cyclic nanoindentation is a robust experimental method that enables an in-depth analysis of how materials behave mechanically under repeated loading conditions. The aim of this study is to utilize the cyclic nanoindentation technique in order to assess the mechanical characteristics, including elastic and plastic deformations, of yttria-stabilized tetragonal zirconia polycrystals (Y-TZP) ceramic material through simulation. A two dimensional Finite Element Analysis (FEA) model is employed to create a nanoindentation simulation with a Berkovich indenter. The cyclic nanoindentation simulation model provides the outcome of the sample's deformation response and the load-displacement curve for each loading cycle of peak load of 500 mN. This model builds upon our previous research with Saedon et al., where we successfully replicated the load-displacement curve obtained by earlier researchers through a single nanoindentation simulation. Given that the sample model is reliable, the results achieved with Y-TZP ceramic are also dependable. In conclusion, this research has successfully replicated the cyclic nanoindentation method using a Berkovich indenter simulation to analyse and understand the mechanical characteristics of Y-TZP ceramic, which is commonly employed in dental prosthetics.

Keywords: FEM, Cyclic nanoindentation, abaqus, Y-TZP ceramic

Nomenclature (Greek symbols towards the end)

E	elastic modulus (GPa)
H_c	contact hardness (GPa)
h_c	contact indentation depth (m)
h_{max}	maximum indentation depth (m)
h_f	final indentation depth (m)
$A(h_c)$	indentation projection area (m^2)
E_r	reduced modulus (GPa)
β	correction factor
S	initial unloading stiffness
dP/dh	slope of the unloading curve
υ	sample's Poisson's ratio
υ_i	indenter's Poisson's ratio
E_i	indenter's elastic modulus (GPa)
H_T	resistance to plastic deformation
h_t	total contact displacement
h_p	plastic displacement
h_e	elastic displacement
α_1	non-dimensional constant for the Berkovich indenter
α_2	Berkovich indenter's geometric constant
E'	plastic strain modulus
ρ_t	theoretical density

Abbreviations

Y-TZP	Yttria-stabilized tetragonal zirconia polycrystals
2-D	2 dimensional
FEA	Finite Element Analysis
CAX4R	a 4-mode bilinear axisymmetric quadrilateral integration element with hourglass control

Received on 19.08.2024
Accepted on 20.09.2024
Published on 27.09.2024

1.0 INTRODUCTION

Accurately defining the properties of materials at the nanoscale is essential for enchancing the functionality and reliability of advanced materials used in various applications. Nanoindentation has emerged as a crucial technique for assessing these characteristics, providing insights toughness, stifness, and other important mechanical properties.

Stabilized zirconia, a ceramic material composed of multiple crystalline phases, is employed as a biomaterial in dental and bone implants [1]. 3Y-TZP, or tetragonal zirconia polycrystal stabilized with yttria, is renowned for its exceptional mechanical properties, including high fracture toughness, strength, and hardness [1]. In dentistry, zirconia with 3 mol% yttria as a stabilizer (3Y-TZP) is commonly used to fabricate crowns and fixed partial dentures [2]. The repairs can be performed either by gently shaping partially sintered blanks prior to high-temperature sintering or by shaping fully sintered blocks with greater force. Yttria-stabilized zirconia was first introduced to the dental industry in 2002 through soft machining [3].

The grain size of 3Y-TZP's significantly influences its mechanical properties. The optimal transformation from tetragonal (t) to monoclinic (m) phases occurs within a narrow range of grain size range of 0.2 μm to 0.8 μm [4]. When the grain size of 3Y-TZP exceeds 1 μm, it becomes less stable and more susceptible to spontaneous t → m transformation. In contrast, grain sizes below 1 μm exhibit a slower transformation rate. Transformation is not feasible at a grain size smaller than approximately 0.2 μm, leading to a reduction in fracture toughness. Controlling grain size is accomplished through sintering, and the conditions during this process significantly affect the stability and mechanical properties of the final product. Higher sintering temperatures and prolonged sintering times result in larger grain sizes [3].

Currently, the 3Y-TZP (3 mol% yttria-stabilized tetragonal zirconia polycrystal) available for the efficient processing of dental restorations is sintered at temperatures ranging from 1350°C to 1550°C, depending on the manuacturer. Soft-machined restorations undergo sintering after the milling process. This approach prevents the stress-induced transformation from tetragonal to monoclinic zirconia, resulting in a robust repair and a surface that are predominantly free of the monoclinic phase, except in areas modified by grinding modifications or sandblasting [5]. Most producers of 3Y-TZP blanks recommend against grinding or sandblasting to avoid the t → m transformation and the deveopment of surface flaws, which could adversely affect performance over time.

On the other hand, restorations produced through hard machining exhibit a significant presence of monoclinic zirconia, often accompanied by surface microcracks, increased susceptibility to low-temperature degradation, and reduced long-term durability [3], [6]. Less frequently used tetragonal zirconia polycrystal (TZPs) contains yttria at concentrations of 4% or 5% mol. Higher yttria levels result in a greater proportion of the cubic phase, which does not convert to the monoclinic phase. Consequently, this produces a ceramic that is highly transparent but possesses weaker mechanical properties due to the absence of transformation toughening [7], [8].

A zirconia dental bridge can sustain damage from frequent biting and minor impacts, resulting in localized contact damage and a reduction in mechanical strength. Therefore, it is crucial to evaluate the susceptibility of zirconia dental ceramics to contact damage in clinical settings. Understanding the mechanical response of Yttria-Stabilized Zirconia (YTZP) ceramics under various loading conditions requires both experimental technique and advanced modeling strategies. Modeling nanoindentation and cyclic nanoindentation processes using two-dimensional Finite Element Analysis (FEA) has proven to be an affective approach. By utilizing the application to nanoindentation, it is possible to examine the distribution of stress and strain fields, in addition to evaluating the load-displacement depth curve. Most importantly, in situations where conventional experimental techniques cannot be performed, numerical simulations can be employed to obtain material model parameters through a back analysis of data from nanoindentation tests. The inverse modeling of non-destructive testing, which is often based on finite element (FE) simulations of the test, appears to be the only viable approach in this context. This is primarily because many researchers have limited access to actual samples or experimental procedures due to costs or geometric constraints.

By employing sophiscated software such as ABAQUS, researchers can create complex computational models to study and pridict how materials respond to different scenarios, including both single and repeated loading conditions. Consequenctly, FEA is frequently utilised to simulate elastic and plastic deformations under a pointed indenter, allowing for the calculation of material properties such as Young's modulus and hardness [9]. The problem is formulated in three dimensions under general conditions. In contrast, for isotropic materials, a comparable conical shape with known geometric properties of conventional tips can be used to define the indenter geometry. The more complex three-dimensional model can be simplified into an axisymmetric one, allowing for numerical solutions in two dimensions. This approach accelerates the nanoindentation back analysis process and streamlines numerical analysis. There are numerous single nanoindentation experiments of zirconia ceramic conducted by previous research; however, it is rare to see the FE simulation of different nanoindentation conditions for zirconia

The aim of this research is to utilise the cyclic nanoindentation method as to assess the mechanical characteristics, such as elastic and plastic deformation, of Y-TZP ceramic material. Additionally, we aim to create a cyclic nanoindentation model simulation with a Berkovich indenter using ABAQUS 6.14 software. To evaluate

the mechanical characteristics, we conducted nanoindentation tests with a peak load of 500 mN over five cycles. A flexible disc material sample was discretized into a small mesh using the axisymmetric element CAX4R and a hard Berkovich indenter was employed at an angle of 70.3 degress.

2.0 METHODOLOGY

2.1 Material Properties

The theoretical density, ρ_t [1] and the reported mechanical properties of Y-TZP materials by Saedon et al. [10], including the Young's modulus and the hardness which where obtained using reversed analysis on load-displacement result by Shao et al. [11], are given in Table 1.

Table 1: Material properties for Y-TZP ceramic sample

Theoretical density	6.08g/cm^3
Young's modulus	319.29 GPa
Material hardness	42.85 GPa

2.2 Model Set Up

The cyclic nanoindentation simulations were conducted using ABAQUS CAE 6.14 (Dassault System, USA). A rigid Berkovich indenter and a 2-D axisymmetric rectangle, with the much larger side length than the indentation depth, were employed to replicate the setup. Since Shao [11] did not specify the size of the zirconia sample, the dimensions of the sample were considered arbitrary; however, the size depicted in Figure 1 is a 60 µm x 40 µm sample. The system exhibits axisymmetry with respect to the central axis (Y-axis) of the indenter. The Berkovich indenter was modeled as rigid surface with an angle of 70.3° and a reference point at the tip. A mesh was created using a CAX4R element in ABAQUS, which is a 4-node bilinear axisymmetric quadrilateral integration element with hourglass control. Regarding the sizes of the specimen and the indenter, the indentation zone was extremely small. A higher concentration of very small meshes was required in the area beneath the indenter to accurately capture the deformation in that region. The elements were gradually enlarged at the opposite end of the sample model by dividing the sample into sections and adjusting the mesh size using seed edge selection. This approach led to the outcome depicted in Fig. 1, where the area under the indentation zone, labeled as A, has a finer mesh size compared to the other end zone, labeled as B. The mesh size at zone A was established through the implementation of the mesh convergence test. This examination assessed the variation in the highest stress level achieved with each mesh size at zone A and the duration required or the nanoindentation simulation to be completed. Table 2 and Fig. 2 present the results of the mesh convergence analysis conducted on the Y-TZP ceramic sample. Since there was no variation in the Von Mises stress level between 50 nm x 50 nm and 100 nm x 100 nm mesh sizes, the latter (100 nm x 100 nm) was selected for the sample due to shorter time required to complete the nanoindentation simulation.

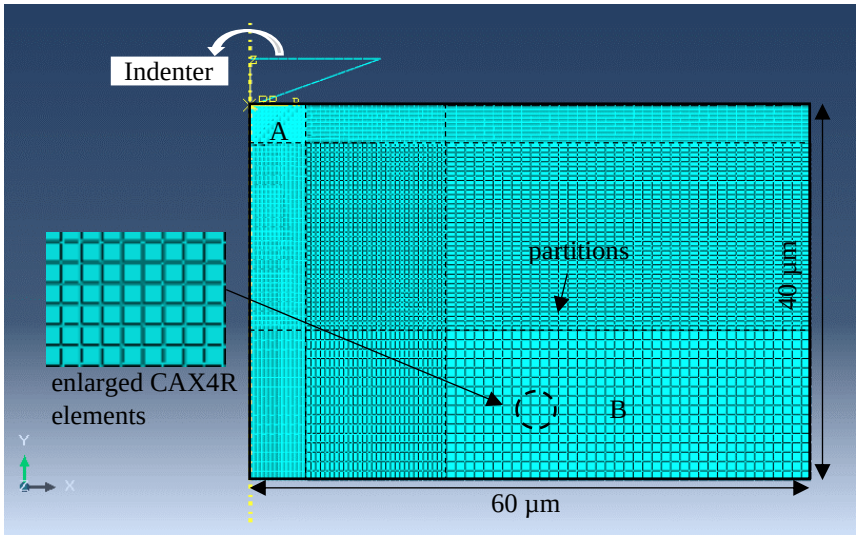

Figure 1. FEM model system with adaptive meshing for Y-TZP ceramic

Table 2: Mesh convergence test for Y-TZP ceramic sample

Mesh size (nm x nm)	Total Element	Converge	Time taken (s)	Von Mises Stress (GPa)
50 x 50	25704	Yes	1080	18.00
100 x 100	12384	Yes	360	18.00
500 x 500	5184	Yes	65	11.95
1000 x 1000	2400	Yes	45	11.45

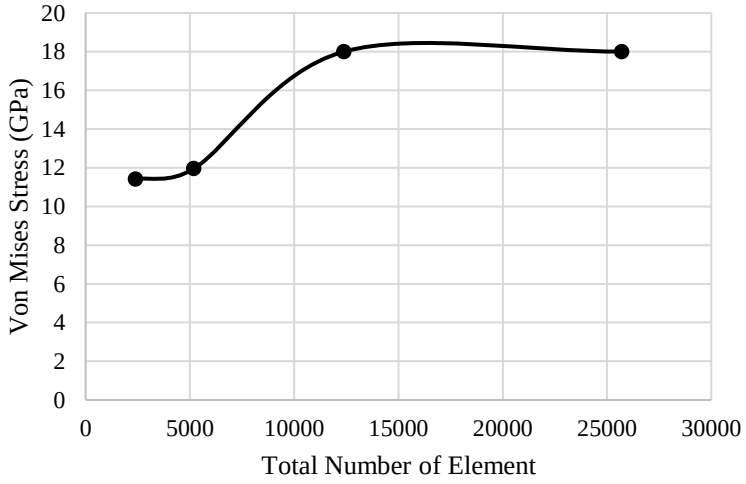

Figure 2. Von Mises Stress vs Total number of element graph

2.3 Application of boundary condition and material parameter

In a previous study co-authored by Saedon et al. [10], the loading and unloading phases of the indenter were controlled by displacing a reference point, which was gradually raised from 0 to h_{max} and then returned to its original position. This process involved the five loading and unloading cycles, with a maximum load of 500 mN applied, followed by a return to 10% of the peak load during each cycle. Consequently, this can be achieved by using load control, where the load was progressively increased from 0 to P_{max}, and an amplitude was assigned to the system. Table 3 provides the guidelines for assigning amplitudes of the five cycles, with the timing adjustable according to the loading rate. Due to its negligible effect on the results, the friction coefficient of the contact was assumed to be zero [12], [13]. To ensure contact between the indenter and the sample, the surface of the indenter was designated as the "master" surface while the surface of the sample was referred as "slave" surface.

To prevent the movement in their normal directions, the nodes at the bottom edges of the sample surface were constrained in all directions using an ENCASTRE boundary condition. At the reference point, the indenter was subjected to a horizontal displacement constraint. To achieve a perfectly plastic simulation, the specimen was assumed to be homogeneous and isotropic.

Table 3: A guideline to assign amplitude for five cycles

	Time	Amplitude
(Start)	0.0	0
	0.5	1
	1.0	0.1
	1.5	1
	2.0	0.1
	2.5	1
	3.0	0.1
	3.5	1
	4.0	0.1
	4.5	1
(End)	5.0	0

2.4 Analysis of indentation properties

The mechanical properties were determined using the Oliver-Pharr method [14] by analysing the load bearing properties produced during nanoindentation. The elastic modulus, E, contact hardness, H_c, contact indentation depth, h_c, the maximum indentation depth, h_{max}, and the final indentation depth, h_f are all the examples of mechanical properties. The contact hardness, denoted as *Hc* can be written as [14]:

$$H_c = \frac{P_{max}}{A(h_c)} \quad \text{(GPa)} \quad (1)$$

where $A(h_c)$ represents the area of indentation projection based on the function of the contact depth, given by the equation $A=24.5(h_c)^2$ [14]. The reduced module can be written as [14]:

$$E_r = \frac{S\beta\sqrt{\pi}}{2\sqrt{A}} \quad \text{(GPa)} \quad (2)$$

where the correction factor, β is approximately 1 with the range of ± 0.05 and S represents the initial unloading stiffness determined by the slope of the unloading curve (dP/dh) at the maximum indentation displacement. The relationship between the young's modulus and the reduced modulus which is defined by Oliver and Pharr [14] is presented as:

$$\frac{1}{E_r} = \frac{1-\upsilon^2}{E} + \frac{1-\upsilon_i{}^2}{E_i} \quad (3)$$

where υ is the Poisson's ratio of the sample, υ_i is the Poisson's ratio of the indenter and E_i is the young's modulus of the indenter.

The Sakai model [15] was utilized to quantify the elastic-plastic behaviour by assessing the resistance to plastic deormation, denoted as H_T, which was determined from the load-displacement curve. In brief, the overall contact displacement, h_t quals the combined plastic h_p and elastic h_e displacement as per following;

$$h_t = h_p + h_e \quad \text{(m)} \quad (4)$$

where the displacements of plastic h_p and elastic h_e can be represented as shown in [16]:

$$h_p = \sqrt{\frac{P_{max}}{\alpha_1 H_T}} \quad \text{(m)} \quad (5)$$

$$h_e = \sqrt{\frac{P_{max}}{\alpha_2 E'}} \quad \text{(m)} \quad (6)$$

hence, Equation (4) can be expressed as;

$$h_t = \sqrt{\frac{P_{max}}{\alpha_2 E'}} + \sqrt{\frac{P_{max}}{\alpha_1 H_T}} \quad \text{(m)} \quad (7)$$

where α_2 for Berkovich indenter's geometric constant is 4.4, E' can be defined as $E/(1-\upsilon^2)$, α_1 as a non-dimensional constant for the Berkovich indenter is 24.5 and H_T denotes the resistance to plasticity as assessed by [11];

$$H_T = \frac{H_c \alpha_2 E'}{\left((\alpha_2 E')^{\frac{1}{2}} - (\alpha_1 H_c)^{\frac{1}{2}}\right)^2} \quad \text{(GPa)} \quad (8)$$

Following to that, the plastic and elastic deformation components can be determined by using Equations (7) and (8) as $h_p/(h_e+h_p)$ and $h_e/(h_e+h_p)$ respectively.

3.0 RESULTS AND DISCUSSION

3.1 Load-displacement curve

In a previous study co-authored by Saedon et al. [10], the simulated nanoindentation was conducted using a displacement control method. However, is it easier to use a load control method in cyclic nanoindentation. Fig. 3 illustrates the comparison between the load versus displacement curves obtained from the displacement control simulation result of Saedon et al. and our load control simulation result of the zirconia sample. The maximum load achieved by the load control method is lower than that obtained with the displacement control method, measuring 487 mN and 493 mN, respectively. To demonstrate the effectiveness of the load control method, Table 2 summarizes the comparison of hardness and Young's modulus values obtained from both simulations and the reference journal of Shao et al. [11]. The results indicate a narrow margin in the percentage error between the load control method and journal, as well as between displacement control method and the journal. This shows evidence that the simulation of load control is also reliable and can be implemented for cyclic nanoindentation.

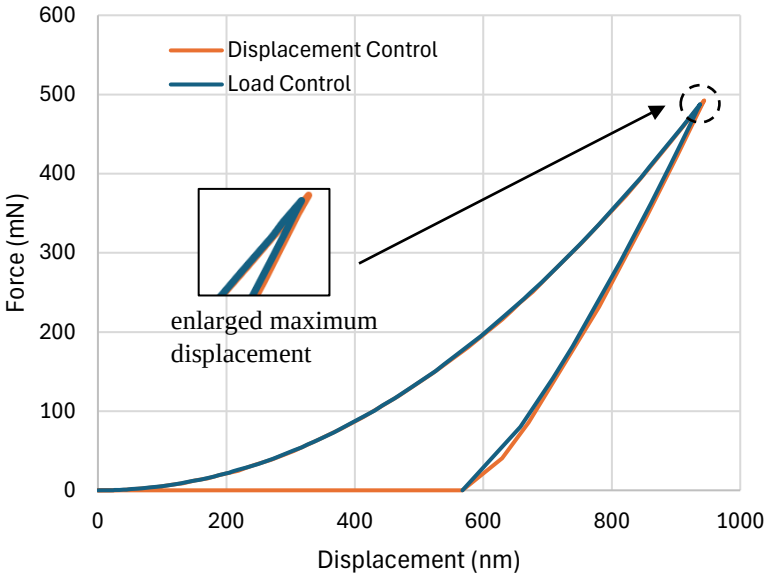

Figure 3. The force-displacement curve of Y-TZP ceramic under with 500 mN peak load using displacement and load control

Table 2. Young's modulus and Hardness Difference

Material	Young's Modulus, E (GPa)	Error (%)	Contact Hardness (GPa)	Error (%)
Ceramic (Y-TZP)	319.29	N/A	42.85	N/A
Simulation (Displacement)	329.54	3.21	44.45	3.73
Simulation (Load)	334.23	4.53	44.06	2.82

Fig. 4 illustrates the force-displacement curve of Y-TZP ceramic subjected to a peak load of 500 mN over 5 loading-unloading cycles. In the initial stages of the peak load depicted in the chart, noticeable differences were observed. Due to the closer proximity of their unloading and reloading curves, subsequent cycles were simpler to replicate. Additional hysteresis loops were generated between the unloading and reloading curves of consecutive cycles.

Fig. 5 shows the maximum depth of indentation, h_{max}, and the contact depth of indentation, h_c, for Y-TZP ceramic compared to the number of cycles they underwent. The Y-TZP indentation reached maximum depths ranging from 925.986 nm to 945.715 nm, while the contact indentation depth varied from 688.527 nm to 698.612 nm.

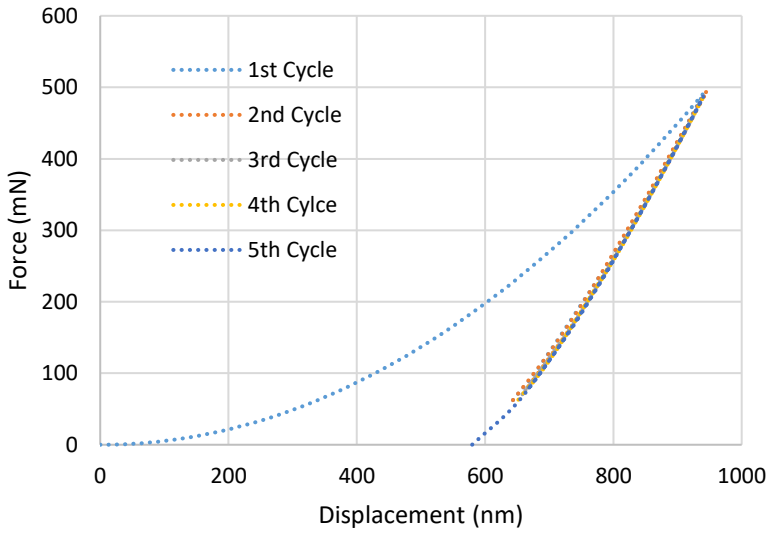

Figure 4. The force-displacement curve of Y-TZP ceramic under with 500 mN peak load for 5 loading-unloading cycles

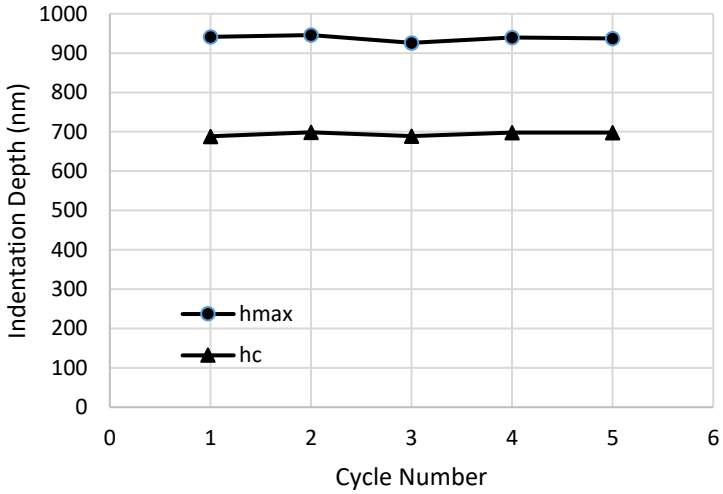

Figure 5. Indentation displacement of maximum depth h_{max} and contact depth h_c for Y-TZP ceramic against nanoindentation cycles

3.2 Mechanical properties and behaviour

Fig. 6 displays the mechanical characteristics of the Y-TZP materials as they underwent various nanoindentation cycles. In Fig. 6a, the Young's moduli (E) exhibited irregular fluations, both increasing and decreasing, as the number of cycle progressed. The moduli of Y-TZP ranged from 345.910 GPa to 352.412 GPa. The contact hardness (Hc), shown in Fig. 6b, also demonstrated a decline in the values as the number of cycles increased, with Y-TZP ceramic hardness ranging from 39.73 GPa to 42.34 GPa. The data presented in Fig. 6c indicated that these values are significantly influenced by the number of cycles, which affects resistance to plastic deformation. Y-TZP has H_T values ranging from 703.79 GPa to 938.34 GPa. In Fig. 6d, there was a slight increase in both plastic and elastic displacement values with the number of cycles for Y-TZP ceramic. Finally, Fig. 6e illustrates the elements of plastic and elastic deformation elements at different cyclic numbers, showing minimal variation in values.

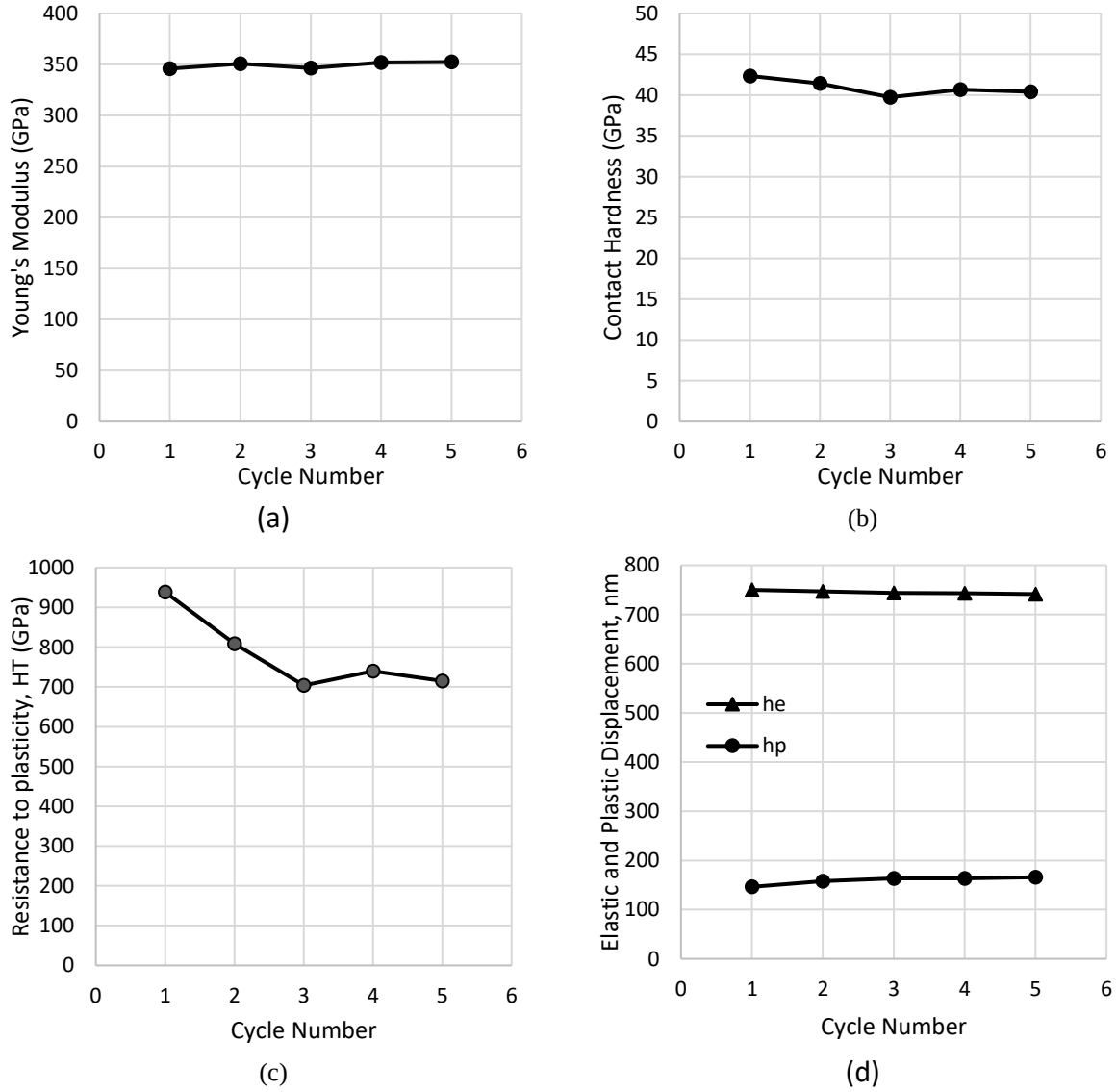

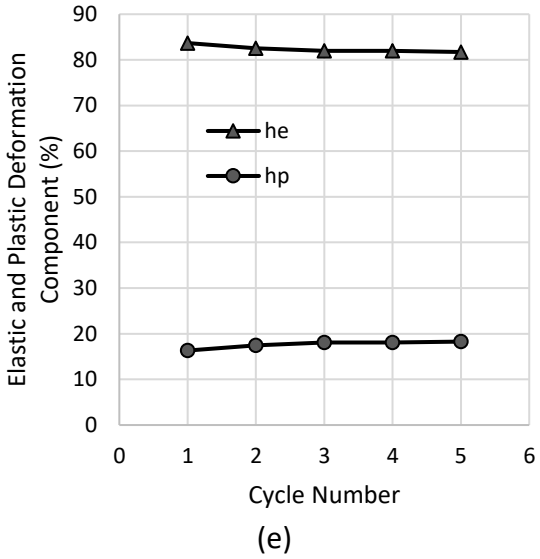

Figure 6. The nanomechanical properties of Y-TZP materials versus nanoindentation cycles, including (a) Young's moduli *E*, (b) contact hardness *Hc*, (c) resistance to plasticity H_T, (d) elastic h_e and plastic h_p displacements, and (e) elastic $h_e/(h_e + h_p)$ and plastic $h_p/(h_e + h_p)$ deformation components

3.3 Discussion

This research employs cyclic nanoindentation to investigate the Young's Modulus, *E*, contact hardness, H_c, resistance to plasticity, H_T, plastic displacement, h_p, elastic displacement, h_e, and plastic deformation component, $h_p/(h_e + h_p)$, as well as the elastic deformation component, $h_e/(h_e + h_p)$ of Y-TZP ceramic. These properties significantly affect the workability of the material, which is crucial for its application in dental restorations.

The relationship between the Young's Modulus and indentation cycles, as illustrated in Fig. 6a may be attributed to the Young's Modulus dependence on the projected area and initial unloading stiffness, as indicated in Equation (2). The initial stiffness during unloading is defined by the first 30% of the depth of unloading. Furthermore, the Y-TZP materials demonstrate quasi-plastic deformation as a result of the indentation. Consequently, the initial unloading stiffness is largely unaffected by this quasi-plastic deformation.

Strain hardening may elucidate how the indentation cycles (Fig. 6b) are influenced by the contact hardness, H_c values. Typically, cyclic pressing results in greater contact depths, which in turn leads to a reduction in hardness as indicated in Equation (1). The load-displacement curves also exhibit these characteristics, with the sample displaying minimal gaps between loading and unloading curves in each cycle (Fig. 6). Accumulated zirconia crystals filling the pores contribute to strain hardening by facilitating zirconia crystal movements and providing resistance to indentation stresses. The material's hardness ratings can offer insights into its fatigue characteristics and limitations.

The value of H_T (Figure 6c) is likely more resistant to plastic deformation due to the components of plastic and elastic deformation components as illustrated in Fig. 6f, which indicates lower plastic and higher elastic deformation components in the former. The Y-TZP ceramic also demonstrates a primary response to plastic deformation. This is evident in the decreasing elastic displacement shown in Fig. 6d and the deformation factor presented in Fig. 6e. Additionally, as the cycle count increases and the plastic deformation component rises, the elastic deformation component decreases (Fig. 6e).

The long-term performance of zirconia materials can be significantly influenced by both manual handpiece adjustment/polishing procedures and dental CAD/CAM milling [17]. Our research indicates that the YTZP zirconia materials exhibit distinct microstructural responses to cyclic nanoindentation, demonstrating quasi-plastic deformation and damage characteristics. The cyclic nano-scale mechanical behaviours are predictive of the machinability and diamond machining mechanisms of zirconia materials. This understanding could provide a foundation in comprehending how zirconia microstructures regulate their mechanical properties, thereby facilitating effective machining techniques for durable zirconia restorations. Fig. 8 illustrates the maximum shear stresses (τmax) in zirconia restorations, both sintered and pre-sintered. The next advancement in zirconia material machinability, which avoids compromising strength due to machining-induced damage, may lie in microstructural design. Furthermore, zirconia products, as load-bearing mechanical components, are susceptible to contact issues which can lead to abrasive wear and erosion; and our data may prove beneficial in this context. Zirconia products may experience catastrophic fatigue failures due to wear damage and stress concentrators resulting from quasi-plastic degradation caused by cyclic indentation.

4.0 CONCLUSION

The research employed nanoindentation to evaluate the mechanical characteristics of ceramic materials, utilizing simulated cyclic nanoindentation with a Berkovich indenter in ABAQUS 6.14. The results from single nanoindentation simulations for the load-displacement curves of the ceramic materials in this study closely align with those reported by earlier researchers. The simulation outcomes indicate that they are influenced by tip radius of the indenter, mesh size, and the hardening law applied to the model. The findings provide insights into how materials respond to repeated impacts, akin to grinding. Material properties deteriorate under cyclic loading. The presence of hysteresis loops and distinct gaps in the load-displacement graphs may be attributed to reversible material changes and the activation of shear planes. The Y-TZP ceramic exhibits plastic deformation when subjected to multiple nanoscale indentations. The mechanical properties and responses observed during nanoindentation may offer insights into the mechanisms of materials removal during small-scale abrasive machining with diamond abrasives. These results establish a foundation for enhancing abrasive machining techinique which contributes to the understanding of the mechanics involved in nanoscale ductile-region material removal. It is essential to investigate the mechanical properties of Y-TZP ceramic, which is widely used in dental prostheses, to prevent potential failures or harm to the individuals using them.

ACKNOWLEDGEMENT

This research was funded by a grant from Universiti Teknologi MARA (600-RMC/GIP 5/3 (009/2022)).

REFERENCES

[1] A. Moradkhani, H. Baharvandi, and A. Naserifar, “Fracture toughness of 3Y-TZP dental ceramics by using Vickers indentation fracture and SelNB methods,” *Journal of the Korean Ceramic Society*, vol. 56, no. 1, pp. 37–48, 2019, doi: 10.4191/kcers.2019.56.1.01.

[2] H. M. Rao, M. Kumaraswamy, D. Thomas, S. Boraiah, and K. S. Rana, “Zirconia in Restorative Dentistry,” in *Zirconia*, U. M. B. Al-Naib, Ed., Rijeka: IntechOpen, 2023, ch. 5. doi: 10.5772/intechopen.111601.

[3] I. Denry and J. A. Holloway, “Ceramics for dental applications: A review,” *Materials*, vol. 3, no. 1, pp. 351–368, 2010, doi: 10.3390/ma3010351.

[4] E. Kontonasaki, A. E. Rigos, C. Ilia, and T. Istantsos, “Monolithic Zirconia: An Update to Current Knowledge. Optical Properties, Wear, and Clinical Performance,” *Dent J (Basel)*, vol. 7, no. 3, 2019, doi: 10.3390/dj7030090.

[5] W. M. Ahmed, T. Troczynski, A. P. McCullagh, C. C. L. Wyatt, and R. M. Carvalho, “The influence of altering sintering protocols on the optical and mechanical properties of zirconia: A review,” *Journal of Esthetic and Restorative Dentistry*, vol. 31, no. 5, pp. 423–430, 2019, doi: https://doi.org/10.1111/jerd.12492.

[6] O. S. Abd El-Ghany and A. H. Sherief, “Zirconia based ceramics, some clinical and biological aspects: Review,” *Future Dental Journal*, vol. 2, no. 2, pp. 55–64, 2016, doi: https://doi.org/10.1016/j.fdj.2016.10.002.

[7] Y. Zhang and B. R. Lawn, “Novel Zirconia Materials in Dentistry,” *J Dent Res*, vol. 97, no. 2, pp. 140–147, 2018, doi: 10.1177/0022034517737483.

[8] A. Y. Alqutaibi *et al.*, “Revolution of Current Dental Zirconia: A Comprehensive Review,” *Molecules*, vol. 27, no. 5, 2022, doi: 10.3390/molecules27051699.

[9] H. Pelletier, J. Krier, A. Cornet, and P. Mille, “Limits of using bilinear stress-strain curve for finite element modeling of nanoindentation response on bulk materials,” *Thin Solid Films*, vol. 379, no. 1–2, pp. 147–155, 2000, doi: 10.1016/S0040-6090(00)01559-5.

[10] J. Saedon *et al.*, “Development of Nanoindentation Simulation Technique for Y-TZP Ceramic Material Characterization,” 2022, pp. 207–216. doi: 10.1007/978-981-19-2890-1_21.

[11] L. Shao, D. Jiang, and J. Gong, “Nanoindentation characterization of the hardness of zirconia dental ceramics,” *Adv Eng Mater*, vol. 15, no. 8, pp. 704–707, 2013, doi: 10.1002/adem.201200367.

[12] A. K. Bhattacharya and W. D. Nix, “Finite element simulation of indentation experiments,” *Int J Solids Struct*, vol. 24, no. 9, pp. 881–891, 1988, doi: 10.1016/0020-7683(88)90039-X.

[13] N. Chollacoop, M. Dao, and S. Suresh, “Depth-sensing instrumented indentation with dual sharp indenters,” *Acta Mater*, vol. 51, no. 13, 2003, doi: 10.1016/S1359-6454(03)00186-1.

[14] G. M. Pharr and W. C. Oliver, “On the generality of the relationship among contact stiffness, contact area and elastic modulus during indentation,” *J Mater Res*, vol. 7, no. 03, 1992.

[15] M. Sakai, “Meyer hardness: A measure for plasticity?,” *J Mater Res*, vol. 14, no. 9, pp. 3630–3639, 1999, doi: 10.1557/JMR.1999.0490.

[16] A. R. Alao and L. Yin, “Assessment of Elasticity, Plasticity and Resistance to Machining-induced Damage of Porous Pre-sintered Zirconia Using Nanoindentation Techniques,” 2016. doi: 10.1016/j.jmst.2016.02.009.

[17] L. Wu, Z. Sun, J. Zhao, and Y. Zheng, “Retrospective clinical study of monolithic zirconia crowns fabricated with a straightforward completely digital workflow,” *Journal of Prosthetic Dentistry*, vol. 128, no. 5, pp. 913–918, Nov. 2022, doi: 10.1016/j.prosdent.2021.01.018.